Article

Ordered Mesoporous Alumina-Supported Metal Oxides

Stacy M. Morris, Pasquale F. Fulvio, and Mietek Jaroniec

More About This Article

Additional resources and features associated with this article are available within the HTML version:

- Supporting Information
- Access to high resolution figures
- Links to articles and content related to this article
- Copyright permission to reproduce figures and/or text from this article

View the Full Text HTML

Ordered Mesoporous Alumina-Supported Metal Oxides

Stacy M. Morris, Pasquale F. Fulvio, and Mietek Jaroniec*

Chemistry Department, Kent State University, Kent, Ohio 44242

Received August 13, 2008; E-mail: jaroniec@kent.edu

Abstract: The one-pot synthesis of alumina-supported metal oxides via self-assembly of a metal precursor and aluminum isopropoxide in the presence of triblock copolymer (as a structure directing agent) is described in detail for nickel oxide. The resulting mesoporous mixed metal oxides possess *p6mm* hexagonal symmetry, well-developed mesoporosity, relatively high BET surface area, large pore widths, and crystalline pore walls. In comparison to pure alumina, nickel aluminum oxide samples exhibited larger mesopores and improved thermal stability. Also, long-range ordering of the aforementioned samples was observed for nickel molar percentages as high as 20%. The generality of the recipe used for the synthesis of mesoporous nickel aluminum oxide was demonstrated by preparation of other alumina-supported metal oxides such as MgO, CaO, TiO_2, and Cr_2O_3. This method represents an important step toward the facile and reproducible synthesis of ordered mesoporous alumina-supported materials for various applications where large and accessible pores with high loading of catalytically active metal oxides are needed.

Introduction

Aluminum oxides are largely studied because of their catalytic,[1−3] optical,[4] electronic,[5] and biomedical properties.[6,7] There has been great interest in obtaining well-defined mesoporous aluminum oxides with high surface area and pore volumes.[1,2,8] Porous aluminum oxides have been synthesized by high-temperature dehydration of bulk powders,[4] aerosol generation of particles with use of block copolymers,[9] modified sol−gel in the presence of organic structural agents,[10,11] cationic[3] and anionic surfactants,[12] block copolymers,[13−15] using ordered mesoporous carbon templates,[16] colloidal precursors with amine structural agents,[17] and evaporation-induced self-assembly (EISA) with block copolymers.[18,19] Also, meso- and macroporous γ-Al_2O_3 was obtained under microwave irradiation in the presence of surfactants under acidic conditions.[20] It is noteworthy that the use of ordered mesoporous carbons as hard templates for the synthesis of mesoporous γ-alumina[16] was an important achievement as it initiated interest in the development of alumina materials with ordered and uniform mesopores. Even though the hard-templating synthesis may afford crystalline aluminas with desired pore geometries and symmetries, this method has several drawbacks. First, it is time consuming because preparation of a carbon template adds additional steps to the synthesis procedure. Also, the nanocasting process consists of several cycles, which often results in a partial or complete loss of mesostructural ordering and the change of particle morphology.

Among various synthesis routes, those employing poly(ethylene oxide)-poly(propylene oxide)-poly(ethylene oxide) block copolymers $[(EO)_x(PO)_y(EO)_x]$ as soft templates attract a lot of attention because they are inexpensive, commercially available, biodegradable, and afford materials with relatively large and uniform mesopores. Early attempts to generate alumina thin films using block copolymers and evaporation-induced self-assembly resulted in amorphous[13] or disordered mesoporous materials with broad pore size distributions.[14] Another strategy employing triblock copolymers as soft templates afforded 3-dimensional (3D) mesoporous structures with disk-shaped pores in the presence of an ammonium hydroxide buffer.[19]

(1) Cejka, J. *Appl. Catal. A: Gen.* **2003**, *254*, 327–338.
(2) Marquez-Alvarez, C.; Zilkova, N.; Perez-Pariente, J.; Cejka, J. *Cat. Rev.-Sci. Eng.* **2008**, *50*, 222–286.
(3) Trueba, M.; Trasatti, S. P. *Eur. J. Inorg. Chem.* **2005**, *17*, 3393–3403.
(4) Fang, X.-S.; Ye, C.-H.; Xu, X.-X.; Xie, T.; Wu, Y.-C.; Zhang, L.-D. *J. Phys.: Condens. Matter* **2004**, *16*, 4157–4163.
(5) Kurien, S.; Mathew, J.; Sebastian, S.; Potty, S. N.; George, K. C. *Mater. Chem. Phys.* **2006**, *98*, 470–476.
(6) Kim, S. E.; Lim, J. H.; Lee, S. C.; Nam, S.-C.; Kang, H.-G.; Choi, J. *Electrochim. Acta* **2008**, *53*, 4846–4851.
(7) Iftekar, S.; Grins, J.; Svensson, G.; Loof, J.; Jarmar, T.; Botton, G. A.; Andrei, C. M.; Engqvist, H. *J. Eur. Ceram. Soc.* **2008**, *28*, 747–756.
(8) Pinnavaia, T. J.; Zhang, Z. R.; Hicks, R. W. *Stud. Surf. Sci. Catal.* **2005**, *156*, 1–10.
(9) Boissiere, C.; Nicole, L.; Gervais, C.; Babonneau, F.; Antonietti, M.; Amenitsch, H.; Sanchez, C.; Grosso, D. *Chem. Mater.* **2006**, *18*, 5238–5243.
(10) Zhao, R.-H.; Li, C. P.; Guo, F.; Chen, J.-F. *Ind. Eng. Chem. Res.* **2007**, *46*, 3317–3320.
(11) Zima, T. M.; Baklanova, N. I.; Lyakhov, N. Z. *Inorg. Mater.* **2008**, *44*, 146–153.
(12) Vaudry, F.; Khodabandeh, S.; Davis, M. E. *Chem. Mater.* **1996**, *8*, 1451–1464.
(13) Yang, P.; Zhao, D.; Margolese, D. I.; Chmelka, B. F.; Stucky, G. D. *Nature* **1998**, *396*, 152–155.
(14) Niesz, K.; Yang, P.; Somorjai, G. A. *Chem. Commun.* **2005**, *15*, 1986–1987.
(15) Zhang, Z.; Pinnavaia, T. J. *J. Am. Chem. Soc.* **2002**, *124*, 12294–12301.
(16) Liu, Q.; Wang, A.; Wang, X.; Zhang, T. *Chem. Mater.* **2006**, *18*, 5153–5155.
(17) Zhang, Z.; Pinnavaia, T. J. *Angew. Chem., Int. Ed.* **2008**, *47*, 7501–7504.
(18) Yuan, Q.; Yin, A.-X.; Luo, C.; Sun, L.-D.; Zhang, Y.-W.; Duan, W.-T.; Liu, H.-C.; Yan, C.-H. *J. Am. Chem. Soc.* **2008**, *130*, 3465–3472.
(19) Kuemmel, M.; Grosso, D.; Boissiere, C.; Smarsly, B.; Brezesinski, T.; Albouy, P. A.; Amenitsch, H.; Sanchez, C. *Angew. Chem., Int. Ed.* **2005**, *44*, 4589–4592.
(20) Ren, T.-Z.; Yuan, Z.-Y.; Su, B.-L. *Langmuir* **2004**, *20*, 1531–1534.

Spherical alumina nanoparticles were prepared by combining the self-assembly of alumina precursors and block copolymers with aerosol formation.[9] Sol−gel methods, which employed diblock and triblock copolymers under basic conditions, afforded mesoporous aluminas with wormhole-like structures.[15]

The first successful synthesis of ordered mesoporous alumina (OMA) in the presence of block copolymers used as soft templates was reported by Niesz et al.;[14] however, this procedure required a strict control of experimental conditions. A major leap in the preparation of γ-Al$_2$O$_3$ with ordered mesopores has been achieved by self-assembly of the $(EO)_{20}(PO)_{70}(EO)_{20}$ triblock copolymer and alumina precursors in ethanolic solution in the presence of additives such as citric or nitric acid.[18] This route has been found to be reproducible and avoids the need for controlling hydrolysis conditions, such as the amount of water and humidity.

Alumina is an important support in catalysis,[1−3] especially now that ordered mesoporous alumina (OMA) can be made in a facile and reproducible manner.[18] Therefore, the recent successful preparation of OMA[18] stimulated us to extend this approach to the one-pot synthesis of alumina-supported metal oxides with well-developed mesoporosity, relatively high surface area, and crystalline pore walls. To illustrate the feasibility of the proposed strategy for the synthesis of alumina-supported metal oxides we present here a systematic study on the synthesis of polymer-templated alumina-supported nickel aluminate because of its importance in catalysis. For instance, nickel aluminate (NiAl$_2$O$_4$) is used as a catalyst for several hydrogenation and dehydrogenation reactions: oxidative dehydrogenation of ethane to ethylene for petrochemical purposes,[21] conversion of methane and carbon dioxide to syngas,[22] and hydrogenation of nitriles.[23] Nickel aluminate is relatively inexpensive compared to other known active catalysts,[22] has strong resistance to acids and bases,[24] and has high thermal stability.[25] Several methods have been employed for the synthesis of NiAl$_2$O$_4$ including wet impregnation of Al$_2$O$_3$,[21] pelletization and sintering of Al$_2$O$_3$ and NiO,[26] as well as those previously discussed. Also, other alumina-supported metal oxides have found various applications: magnesium aluminum oxide is used as a refractory material[27] and in sensors and electronic devices;[28] calcium aluminum oxide is used in high-strength industrial and dental cements, flame detectors,[29] and as hydraulic materials;[27] titanium aluminum oxide is used as a potential adsorbent in the chemical decontamination of chemical warfare agents,[30] in materials for aeronautical and automotive purposes,[31] and in orthopedic and dental implants;[32] and chromium aluminum oxide is used as temperature sensors[33] and for dehydrogenation of alkanes.[34] To the best of our knowledge, there is no report on the one-pot synthesis of crystalline alumina-supported metal oxides with ordered mesoporosity.

The aforementioned strategy permits the one-pot synthesis of various alumina-supported metal oxides. The potential of this synthesis strategy to achieve high loadings of metal oxides in mesoporous alumina is illustrated through a detailed study of the alumina−nickel oxide system. Additionally, its generality is demonstrated by the preparation of various alumina-supported metal oxides such as MgO, CaO, TiO$_2$, and Cr$_2$O$_3$. These alumina samples with up to 20% metal oxide loading exhibited ordered mesoporosity as evidenced by small angle XRD and TEM analysis, relatively high degree of crystallinity, and a homogeneous distribution of metal oxide as evidenced by in situ EDX analysis. These materials were thermally stable up to 900 °C, which was reflected by preserving their mesoporous nature during the growth of nanocrystalline double oxide phases with the spinel-type structure confirmed by wide angle powder XRD patterns. All samples studied possessed large and uniform mesopores, as well as high specific surface areas, as obtained from nitrogen adsorption isotherms at −196 °C. The aforementioned recipe represents an important step toward the synthesis of ordered alumina-supported ceramic materials for various applications where large and accessible mesopores with a high loading of catalytically active metal oxides are required.

Experimental Section

**Synthesis of γ-Aluminum Oxide and Mixed Aluminum Oxide Powders.** Alumina powders were synthesized using a similar procedure to that reported by Yuan and co-workers.[18] Approximately 2.0 g of $(EO)_{20}(PO)_{70}(EO)_{20}$ triblock copolymer (Pluronic P123 from BASF, Co.) was dissolved in 20.0 mL of 99.5+% anhydrous ethanol, 200 proof (Acros Organics), and allowed to stir for 4 h. Then, approximately 20 mmol of 98+% aluminum isopropoxide (Acros Organics) was dissolved in 3.2 mL of 68−70 wt % nitric acid (Acros Organics) and 10.0 mL of anhydrous ethanol. Once dissolved, the two solutions were combined and 10.0 mL of anhydrous ethanol was used to thoroughly transfer the aluminum isopropoxide solution. The combined solution was allowed to continue stirring for 5 h. Solvent evaporation was performed at 60 °C for 48 h in air without stirring.

The resulting samples were calcined at 400, 700, and 900 °C in a horizontal quartz tube furnace with a heating rate of 1 °C/min and held at the final temperature for 4 h. Calcinations at 1100 °C were performed in a stepwise manner with a first step to 400 °C with a heating rate of 1 °C/min and a second step to 1100 °C with a heating rate of 5 °C/min, in addition, 1 h hold time was applied at 400 and 1100 °C. All calcinations were performed in flowing air.

A systematic study of nickel aluminum oxide was prepared at various molar fractions of nickel to aluminum. The nickel precursor, nickel(II) nitrate hexahydrate (99%; Acros Organics), was dissolved with the P123 triblock copolymer template in anhydrous ethanol with the remaining synthesis as described above for pure alumina. The total quantity of metal species (20 mmol) was kept constant, and the ratio of nickel to aluminum was adjusted accordingly (5%, 10%, 20%, 33%, 50%).

(21) Heracleous, E.; Lee, A. F.; Wilson, K.; Lemonidou, A. A. *J. Catal.* **2005**, *231*, 159–171.

(22) Zhang, S.; Wang, J.; Liu, H.; Wang, X. *Catal. Commun.* **2008**, *9*, 995–1000.

(23) Salagre, P.; Fierro, J. L. G.; Medina, F.; Sueiras, J. E. *J. Mol. Catal. A: Chem.* **1996**, *106*, 125–134.

(24) Cesteros, Y.; Salagre, P.; Medina, F.; Sueiras, J. E. *Chem. Mater.* **2000**, *12*, 331–335.

(25) Utchariyajit, K.; Gulari, E.; Wongkasemjit, S. *Appl. Organomet. Chem.* **2006**, *20*, 81–88.

(26) Han, Y. S.; Li, J. B.; Ning, X. S.; Yang, X. Z.; Chi, B. *Mater. Sci. Eng., A* **2004**, *369*, 241–244.

(27) Narayanan, R.; Laine, R. M. *Appl. Organomet. Chem.* **1997**, *11*, 919–927.

(28) Kang, Y. C.; Choi, J. S.; Park, S. B. *J. Eur. Ceram. Soc.* **1998**, *18*, 641–646.

(29) Mercury, J. M.; De Aza, A. H.; Pena, P. *J. Eur. Ceram. Soc.* **2005**, *25*, 3269–3279.

(30) Wagner, G. W.; Procell, L. R.; Munavalli, S. *J. Phys. Chem. C* **2007**, *111*, 17564–17569.

(31) Mas-Guindal, M. J.; Benko, E.; Rodriguez, M. A. *J. Alloys Compd.* **2008**, *454*, 352–358.

(32) Kim, S. E.; Lim, J. H.; Lee, S. C.; Nam, S.-C.; Kang, H.-G.; Choi, J. *Electrochim. Acta* **2008**, *53*, 4846–4851.

(33) Pflitsch, C.; Siddiqui, R. A.; Eckert, C.; Atakan, B. *Chem. Mater.* **2008**, *20*, 2773–2778.

(34) Snytnikov, V. N.; Stoyanovskii, V. O.; Larina, T. V.; Krivoruchko, O. P.; Ushakov, V. A.; Parmon, V. N. *Kinet. Catal.* **2008**, *49*, 291–298.
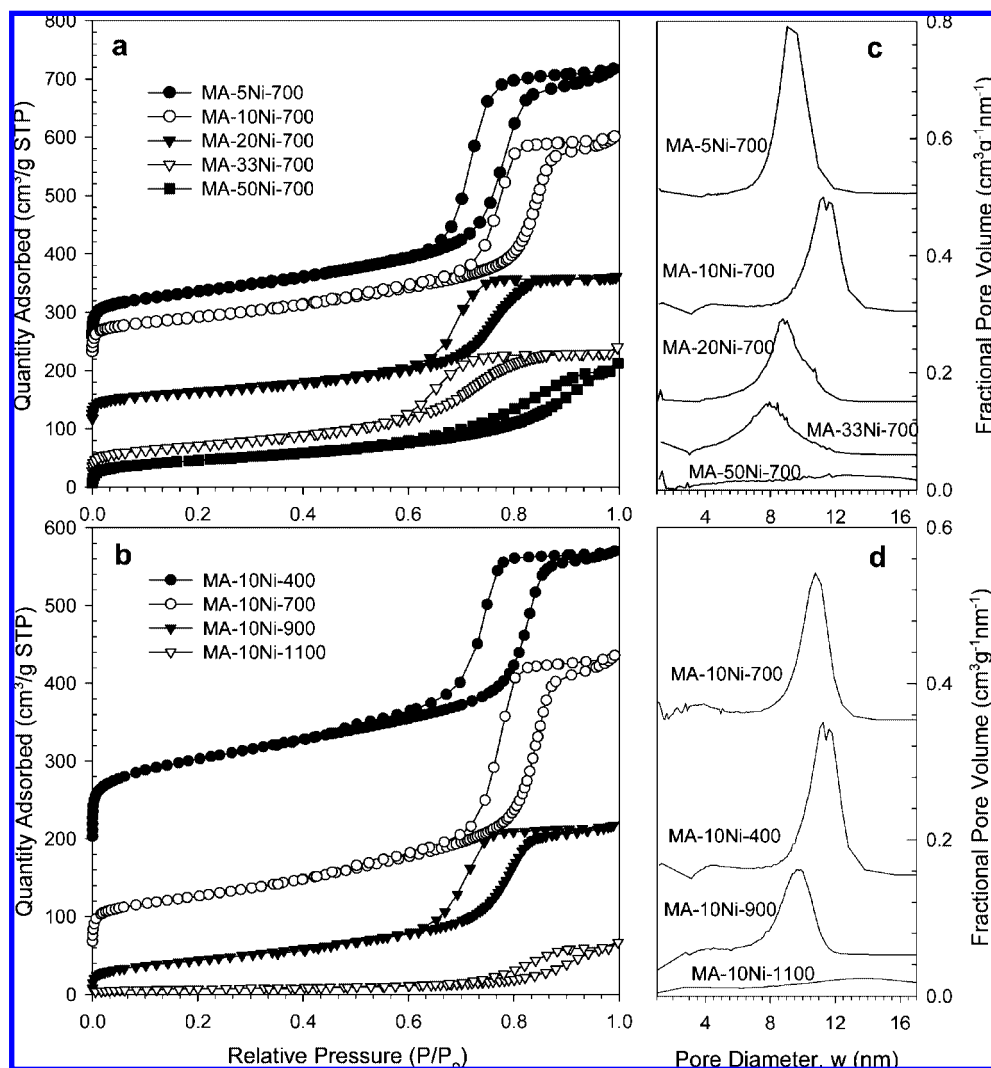
Figure 1. Adsorption isotherms (a and b) and the corresponding pore size distributions (c and d) for mesoporous aluminum oxide samples with differing molar fractions of nickel and aluminum and calcined at 700 °C (a and c) and mesoporous aluminum oxide samples with 10% nickel calcined at different temperatures (b and d). The isotherms (a) for MA-5Ni-700, MA-10Ni-700, MA-20Ni-700, and MA-33Ni-700 were offset by 250, 225, 100, and 25 cm^3/g STP, respectively, and isotherms (b) for MA-10Ni-400, MA-10Ni-700, and MA-10Ni-1100 were offset by 195, 60, and 10 cm^3/g STP, respectively. The pore size distributions (c) for MA-5Ni-700, MA-10Ni-700, MA-20Ni-700, and MA-33Ni-700 were offset by 0.50, 0.30, 0.15, and 0.06 cm^3 g^{-1} nm^{-1}, respectively, and those (d) for MA-10Ni-400, MA-10Ni-700, MA-10Ni-900, and MA-10Ni-1100 were offset by 0.35, 0.15, 0.05, and 0.01 cm^3 g^{-1} nm^{-1}, respectively.

In order to illustrate the generality of this approach, a series of alumina-supported metal oxide samples was synthesized in which a 10% molar fraction of Al was substituted with a metal (Mg, Ca, Ti, or Cr). Precursors for magnesium–, calcium–, titanium–, and chromium−aluminum oxides were 98+% magnesium nitrate hexahydrate (Acros Organics), 99+% calcium nitrate tetrahydrate (Acros Organics), 98+% titanium(IV) isopropoxide (Acros Organics), and 99+% chromium chloride (Matheson, Coleman, and Bell), respectively. For titanium−aluminum mixed oxide, the Ti-containing precursor was added to the P123 solution after addition of aluminum isopropoxide.

The final materials were labeled starting with mesoporous alumina (MA) followed by metal molar percentage (*x*), type of metal substituting alumina (Me), and finally calcination temperature (*T*) in the general form MA-*x*Me-*T*. For instance, MA-10Ni-700 refers to a mesoporous aluminum oxide sample with 10% molar fraction of nickel calcined at 700 °C for 4 h in air.

Measurements and Characterization. Powder X-ray diffraction (XRD) measurements were performed using an X'Pert Pro MPD multipurpose diffractometer (PANalytical, Inc.) with Cu Kα radiation (0.15406 nm) at room temperature from 20.0° to 80.0°

(wide angle) and 0.4° to 5.0° (small angle). Measurements were conducted using a voltage of 40 kV, current setting of 40 mA, step size of 0.02°, and count time of 4 (wide angle) and 20 s (small angle). Microscope glass slides were used as sample supports for all samples.

Nitrogen adsorption measurements were performed using ASAP 2010 and ASAP 2020 (Micromeritics, Inc.) volumetric analyzers at −196 °C with ultra-high-purity nitrogen gas. All samples were outgassed under vacuum at 200 °C for 2 h prior to measurement.

Thermogravimetric (TG) measurements were rendered on a TA Instruments TGA 2950 thermogravimetric analyzer. TG profiles were recorded up to 800 °C in flowing air with a heating rate of 5 °C/min using a high-resolution mode. Elemental analysis was carried out on a LECO model CHNS-932 elemental analyzer.

^{27}Al MAS-NMR was performed on a Bruker DMX NMR spectrometer with 4 mm ZrO_2 rotors, spun at 6 and 7 KHz. Single excitation pulse experiments were performed with an 18° pulse width of 0.9 μs and a relaxation delay of 2 s. The chemical shifts were referenced to an $AlCl_3$ solution.

Samples were imaged by a Hitachi HD-2000 scanning and transmission electron microscope (STEM). For the STEM analysis,

Table 1. Adsorption Parameters for the Ni-Containing Alumina Samples Studied, Obtained by Analysis of Nitrogen Adsorption Isotherms and the Corresponding Pore Size Distributions[a]

sample	S_{BET} (m²/g)	V_{sp} (cm³/g)	V_c (cm³/g)	w_{KJS} (nm)
MA-400	228	0.41	0.00	8.25
MA-700	292	0.62	0.01	9.06
MA-900	222	0.46	0.00	8.10
MA-1100	10	0.05	0.00	0.00
MA-5Ni-400	268	0.47	0.00	8.27
MA-5Ni-700	306	0.71	0.00	9.04
MA-5Ni-900	204	0.36	0.01	7.58
MA-5Ni-1100	15	0.07	0.00	12.80
MA-10Ni-400	385	0.57	0.03	10.78
MA-10Ni-700	237	0.57	0.01	11.26
MA-10Ni-900	160	0.33	0.00	9.63
MA-10Ni-1100	26	0.09	0.00	13.58
MA-20Ni-400	326	0.51	0.01	8.76
MA-20Ni-700	193	0.38	0.00	8.78
MA-20Ni-900	143	0.29	0.00	8.13
MA-20Ni-1100	40	0.05	0.00	12.00
MA-33Ni-400	247	0.36	0.01	8.11
MA-33Ni-700	186	0.32	0.00	7.94
MA-33Ni-900	102	0.17	0.00	8.44
MA-33Ni-1100	8	0.02	0.00	11.16
MA-50Ni-400	253	0.40	0.02	13.50
MA-50Ni-700	168	0.31	0.02	12.43
MA-50Ni-900	40	0.14	0.00	12.87
MA-50Ni-1100	13	0.05	0.00	17.92

[a] V_{sp} = single-point pore volume calculated from the adsorption isotherm at P/P_o = 0.98; S_{BET} = BET specific surface area obtained from adsorption data in the P/P_o range from 0.05 to 0.2; V_c = complementary pore volume calculated by integration of the PSD curve up to ∼3 nm; w_{KJS} = pore width calculated at the maximum of PSD.

the sample powders were dispersed in ethanol by moderate sonication at concentrations of 5 wt % solids. A Lacy carbon-coated, 200-mesh, copper TEM grid was dipped into the sample suspension and then dried under vacuum at 80 °C for 12 h prior to analysis. The unit was operated at an accelerate voltage of 200 kV and an emission current of 30 mA. The energy dispersive spectra (EDX) were collected in tandem by a detector that acquires signals from the selected sample area. The EDX spectra were collected at 30% of detector dead time and 3 min acquisition time.

Calculations. Adsorption parameters for samples were determined from the nitrogen adsorption data collected. The specific surface areas (S_{BET}) were calculated using the BET method in the
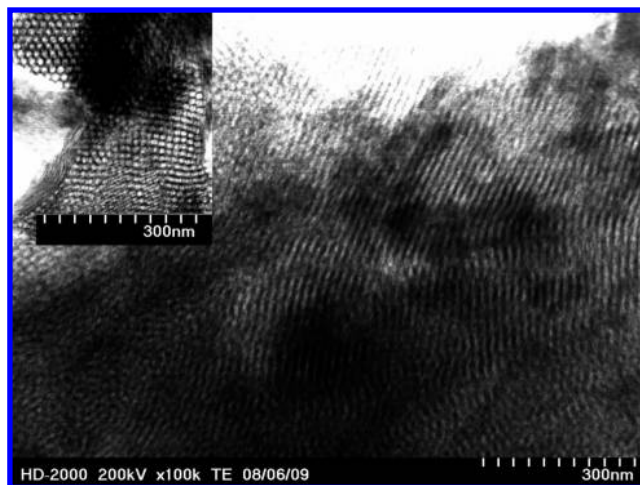
Figure 3. TEM image for MA-10Ni-700. Inset displays honeycomb structure of mesopores.

relative pressure range of 0.05−0.2.[35] The single-point pore volume (V_{sp}) was calculated from the adsorption isotherm at a relative pressure of 0.98. Pore size distributions (PSDs) were calculated using adsorption branches of nitrogen adsorption−desorption isotherms by the improved KJS method calibrated for cylindrical pores.[36] The pore width (w_{KJS}) was obtained at the maximum of the PSD curve. The complementary pore volume, V_c, was evaluated by integration of the PSD curve up to ∼3 nm.

Results and Discussion

Nitrogen adsorption isotherms for a series of nickel aluminum oxide samples calcined at 700 °C with increasing molar fraction of nickel are shown in Figure 1a. All isotherms are type IV with H1 hysteresis loops characteristic for mesoporous materials.[35] The steepness of the capillary condensation step indicates uniformity of mesopores. As can be seen from Figure 1a a decrease in the steepness of the capillary condensation step is observed with increasing molar fraction of nickel (from MA-5Ni-700 to MA-50Ni-700). The condensation step for MA-10Ni-700 is slightly shifted to greater relative pressures, indicating larger mesopores. MA-50Ni-700 contains an excess of Ni in
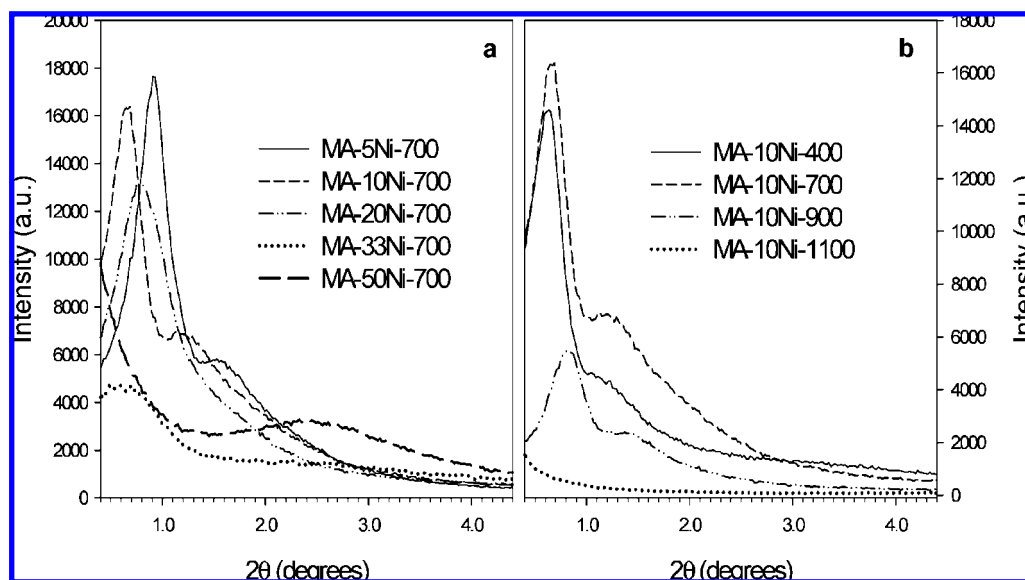
Figure 2. Small angle XRD patterns for mesoporous nickel−aluminum oxide samples with differing molar fractions of nickel and aluminum calcined at 700 °C (a) and patterns for mesoporous alumina samples with 10% nickel oxide calcined at different temperatures (b).
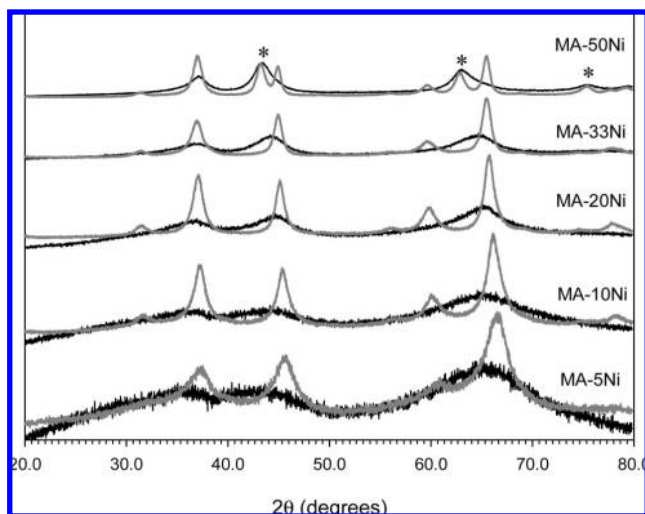
Figure 4. Powder XRD patterns for mesoporous Ni-containing aluminum oxide samples with different molar fractions of Ni. The black and gray lines refer to the samples calcined at 700 and 900 °C, respectively. XRD patterns for the samples calcined at 900 °C were assigned as follows: MA-5Ni (η-alumina, JCPDS 1-77-396), MA-10Ni (η-alumina, JCPDS 1-77-396 and $NiAl_2O_4$, JCPDS 1-81-716), MA-20Ni ($NiAl_2O_4$, JCPDS 1-78-2181), MA-33Ni ($NiAl_2O_4$, JCPDS 1-71-963), and MA-50Ni ($NiAl_2O_4$, JCPDS 1-78-2181 and NiO, JCPDS 22-1189). Asterisks denote peaks characteristic of NiO in MA-50Ni.
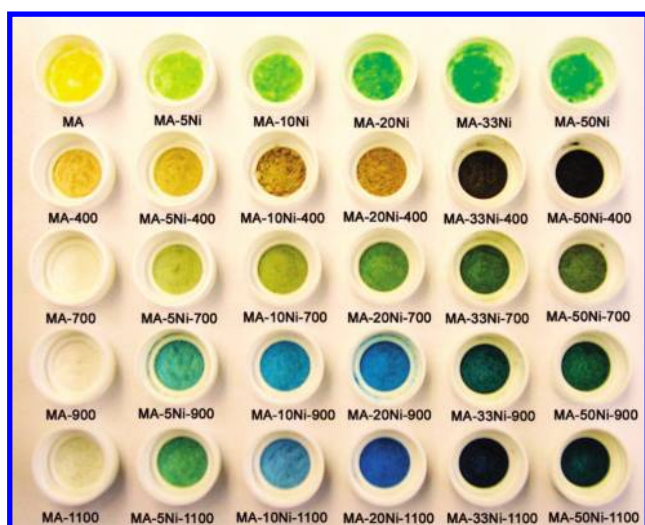
Figure 5. Photograph of pure alumina and nickel-containing aluminum oxides.

comparison to the Ni/Al molar ratio characteristic for nickel aluminate ($NiAl_2O_4$), which results in disordered and much larger mesopores than those present in the remaining samples of this series. However, up to the stoichiometric quantity of nickel added (MA-33Ni-700), the samples display uniformity and large mesopores.

Figure 1b displays the nitrogen adsorption isotherms for 10% nickel aluminum oxide calcined at different temperatures from 400 to 1100 °C. Again, all samples are type IV isotherms with H1 hysteresis loops characteristic for mesoporous materials.[35] Except for the isotherm for MA-10Ni-1100, the other isotherms exhibit steep capillary condensation steps which indicate uniformity of mesopores. Among the latter three samples the condensation step for MA-10Ni-700 is shifted to higher relative pressures, indicating larger mesopores. Also, the isotherm for MA-10Ni-700 shows a greater and steeper condensation step,

indicating a larger volume of primary mesopores (see Table 1) and their higher uniformity. For the sample calcined at 1100 °C (MA-10Ni-1100) the small adsorption quantity and broad capillary condensation step indicate a substantial collapse of ordered mesoporosity.

Shown in Figure 1c and 1d are the pore size distributions for the Ni-containing alumina samples studied. For the adsorption isotherms with steep condensation steps (e.g., MA-5Ni-700, MA-10Ni-700), the corresponding PSD curves represent narrow distributions; however, isotherms with broader condensation steps (e.g., MA-33Ni-700, MA-10Ni-900) also generate broader pore size distributions. Adsorption isotherms and PSDs for Ni-containing samples are similar to the corresponding pure alumina samples (see Figures S1–S3 in the Supporting Information).

The pore widths (w_{KJS}) evaluated at the maximum of the PSD curves are listed in Table 1. As can be seen from this table the dependence of the pore width on the calcination temperature is quite complex for the Ni-containing alumina samples; for the samples with up to 20% of Ni this behavior is analogous as in the case of pure aluminum oxide.[18] Namely, an increase in the calcination temperature from 400 to 700 °C causes an increase in the pore width followed by a decrease and subsequent increase in the pore width for calcinations at 900 and 1100 °C, respectively. An initial increase in the pore width for the samples calcined at 700 °C is due to sample densification associated with local crystallization; analogous behavior was reported for pure alumina samples.[37] Calcination at higher temperatures (~900 and 1100 °C) caused a reduction of the pore width due to shrinkage of the structure; however, its enlargement was caused by collapse of the structure associated with formation of larger irregular mesopores. For samples with a Ni loading of 33% and higher, disordered porosity is observed and the aforementioned changes are even more complex.

Except for pure alumina and 5% Ni-containing samples, the BET surface area and pore volume decrease with increasing calcination temperature (see Table 1). In the case of the aforementioned MA and MA-5%Ni samples, a maximum in the surface area and pore volume is observed at a calcination temperature of 700 °C. In general, an increase in the Ni loading up to 20% does not cause significant changes in the surface area and pore volume for the samples studied. A noticeable reduction of these values is observed for Ni loadings exceeding 33%. An interesting behavior is observed for the BET surface area of the samples calcined at 400 °C; initially this parameter increases with increasing Ni loading to reach a maximum at 10% of Ni followed by its gradual decrease with further increase of Ni loading; also, the BET surface areas of all Ni-containing alumina samples listed in Table 1 are greater than that for pure alumina. This effect gradually disappears for the samples calcined at higher temperatures. Another interesting feature of the samples studied is a very small volume of fine (complementary) pores, which contrast these materials in comparison with their polymer-templated silica counterpart, SBA-15.[38]

Evidence of the presence of hexagonally ordered mesopores (*p6mm* symmetry) for the Ni-containing alumina samples is provided by small angle XRD patterns (Figure 2) and TEM images (Figure 3). The XRD patterns for MA-5Ni-700, MA-

(35) Kruk, M.; Jaroniec, M. *Chem. Mater.* **2001**, *13* (10), 3169–3183.
(36) Jaroniec, M.; Solovyov, L. *Langmuir* **2006**, *22*, 6757–6760.
(37) Pena-Gonzalez, V.; Diaz, I.; Marquez-Alvarez, C.; Sastre, E.; Perez-Pariente, J. *Microporous Mesoporous Mater.* **2001**, *44–45*, 203–210.
(38) Ryoo, R.; Ko, Ch. H.; Kruk, M.; Antochshuk, V.; Jaroniec, M. *J. Phys. Chem. B* **2000**, *104*, 11465–11471.
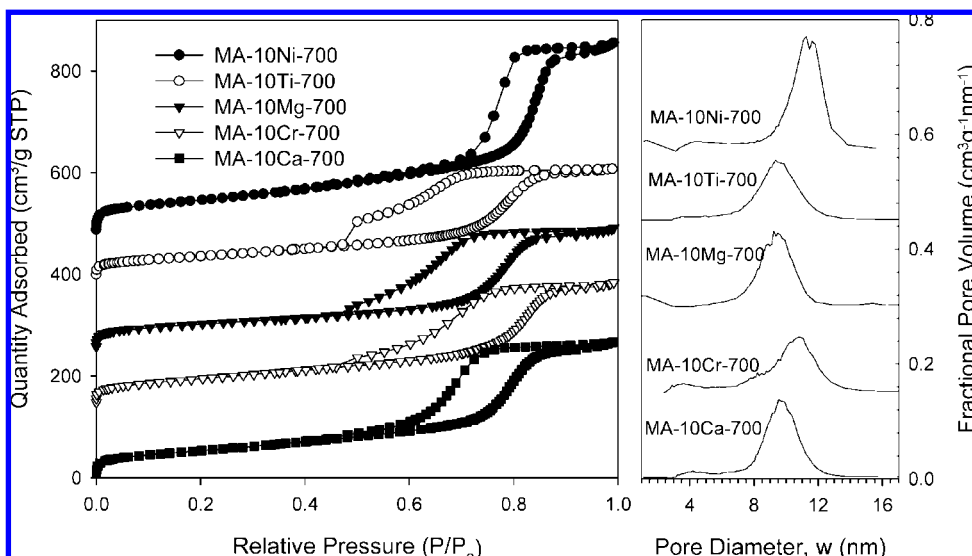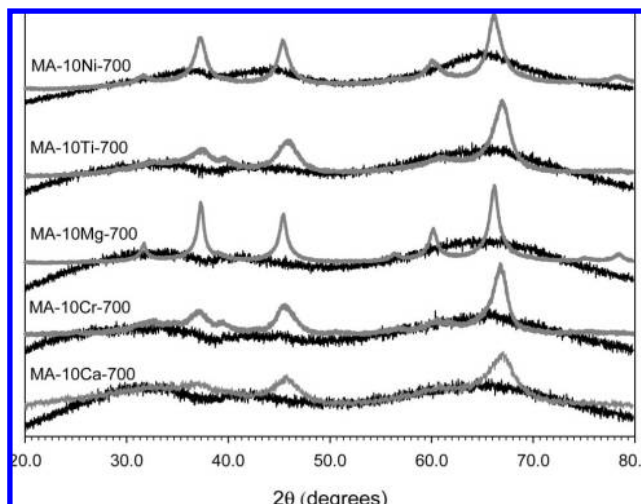
Figure 6. Nitrogen adsorption isotherms (left) and PSDs (right) for 10% metal-containing aluminum oxides. The isotherms for MA-10Ni-700, MA-10Ti-700, MA-10Mg-700, and MA-10Cr-700 were offset by 480, 390, 250, and 140 cm^3/g STP, respectively. PSDs for MA-10Ni-700, MA-10Ti-700, MA-10Mg-700, and MA-10Cr-700 were offset by 0.57, 0.45, 0.30, and 0.15 cm^3 g^{-1} nm^{-1}, respectively.
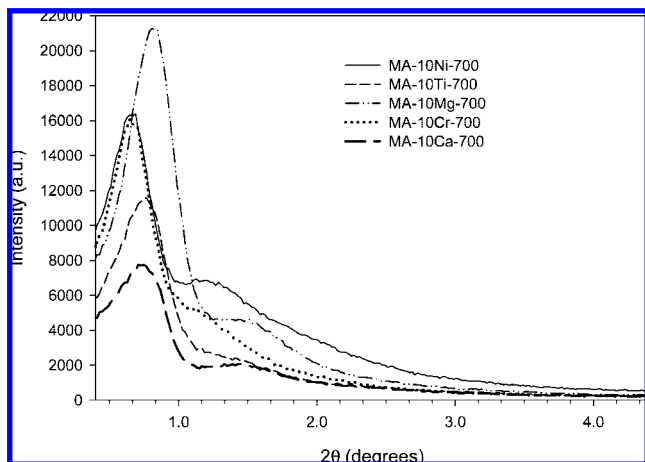
Figure 7. Small angle XRD patterns for 10% Me-containing aluminum oxide samples calcined at 700 °C, where Me = Ni, Mg, Ca, Ti, and Cr.

Figure 8. Wide angle XRD patterns for 10% Me-containing aluminum oxide samples calcined at 700 (black lines) and 900 °C (gray lines), where Me = Ni, Mg, Ca, Ti, and Cr.

10Ni-700, and MA-20Ni-700 clearly show a strong (100) peak (associated with the *d*-spacing values of 8.02, 10.86, and 8.91 nm, respectively). Also, for the first two samples the (110) peak is clearly visible in Figure 2a. In the case of MA-33Ni-700, one broad XRD peak corresponding to *d* = 9.37 nm is visible. Figure 2b displays small angle XRD patterns for MA-10Ni samples calcined at different temperatures. The XRD patterns show two reflections, (100) and (110), for the MA-10Ni samples calcined at 400, 700, and 900 °C; the *d*-spacing values corresponding to (100) reflections are 10.77 nm for MA-10Ni-400, 10.86 nm for MA-10Ni-700, and 8.69 nm for MA-10Ni-900. The XRD spectrum for MA-10Ni-1100 is featureless, indicating the lack of ordered porosity.

The presence of uniform and hexagonally ordered mesopores with *p6mm* symmetry for samples up to 20% nickel was confirmed by TEM analysis (see Figure 3 and Supporting Information Figure S4 showing images for MA-10Ni-700). The small inset in Figure 3 exhibits the characteristic honeycomb structure for *p6mm* symmetry group. This finding is in full agreement with the images of pure alumina sample synthesized

for the purpose of comparison (Figure S5 in the Supporting Information) and the aforementioned article devoted to OMA synthesis.[18]

EDX measurements (Figure S6 in the Supporting Information) indicate a homogeneous distribution of Ni and Al species throughout the entire periodic mesostructure (mixed oxide phase) instead of isolated single oxide domains. In addition, solid-state ^{27}Al NMR spectra (Figure S7 in the Supporting Information) for MA-10Ni samples indicate that nickel replaced tetrahedrally coordinated aluminum (observed in alumina samples), giving nickel aluminate.[18,39] The corresponding NMR spectra for pure alumina samples show the presence of tetrahedral-, pentahedral-, and octahedral-coordinated aluminum and the gradual disappearance of pentahedral aluminum at higher calcination temperatures. In contrast, the spectra for MA-10Ni show pentahe-

(39) Deng, W.; Bodart, P.; Pruski, M.; Shanks, B. H. *Microporous Mesoporous Mater.* **2002**, *52*, 169–177.

dral- and octahedral-coordinated aluminum with the former disappearing at higher calcination temperatures.

Wide angle powder XRD patterns (Figure 4 and Figure S8 in the Supporting Information) for Ni-containing alumina samples calcined at 900 and 1100 °C confirm the presence of $NiAl_2O_4$ in all of the samples except for MA-5Ni-900. As the molar fraction of nickel increases in the samples, the peaks shift from a typical aluminum oxide pattern to those of $NiAl_2O_4$ (see Figure 4 caption). The wide angle XRD patterns for MA-5Ni-900 and MA-10Ni-900 display rapidly decreasing quantities of Al_2O_3, which is not visible for samples with a nickel content above 20%, most likely due to overlapping of alumina and the most intense $NiAl_2O_4$ peaks. The XRD pattern for MA-50Ni-900 contains peaks (43.3°, 62.9°, and 75.5°; see asterisks in Figure 4) that indicate the presence of NiO in addition to $NiAl_2O_4$. The presence of $NiAl_2O_4$ peaks and absence of individual Al_2O_3 and NiO phases support evidence that the latter phases were homogeneously mixed. Samples calcined at 700 °C begin to display crystallinity, and those calcined at 900 °C are crystalline samples as supported by the powder XRD patterns with distinctive peaks. These samples are thermally stable and can be calcined up to 900 °C while maintaining large pores, large surface area, crystallinity, and uniform ordered mesoporosity, although calcination at 700 °C appears to be ideal for maintaining favorable adsorption characteristics and obtaining materials with some degree of crystallinity. Samples calcined at 1100 °C are highly crystalline (see Figure S8 in the Supporting Information), but their pore volume and surface area are very small due to significant structure collapse.

At lower calcination temperatures (400 and possibly 700 °C) there may be Ni_2O_3 present in addition to NiO. Figure 5 shows a photograph of all alumina and Ni-containing aluminum oxides. Samples calcined at 400 °C are increasingly dark from 0 to 50% of Ni. Al_2O_3 is white,[18] $NiAl_2O_4$ is bright blue-green,[25] NiO is green, Ni_2O_3 is grayish-black,[40] and a mixture of NiO and Ni_2O_3 has been described as brownish in color.[41] Wide angle XRD patterns in Figure 4 provide evidence for the presence of NiO in MA-50Ni-700 and -900 but do not show evidence for Ni_2O_3. Elemental analysis was performed for all samples calcined at 400 and 700 °C to determine if carbon from the triblock copolymer was still present in the samples in order to explain the dramatic color change. There was no more than 1% wt carbon found in any of the samples and less than or equal to 0.65% wt carbon in samples calcined at 700 °C. Probably at lower calcination temperatures there is a mixture of small amounts of NiO and Ni_2O_3 (not detectable by XRD), which at higher calcination temperatures converts to NiO (as seen in Figure 4). Conversion of Ni_2O_3 to NiO at higher temperatures has been previously reported.[40,41]

To demonstrate the applicability of the proposed approach to the synthesis of other alumina-supported metal oxides, alumina samples containing magnesium, calcium, titanium, and chromium oxides were prepared and characterized analogously as in the case of aluminum–nickel mixed oxides. Figures 6 and 7 show nitrogen adsorption isotherms with the corresponding

PSDs and small angle XRD patterns, respectively, for alumina samples containing 10% of the aforementioned oxides calcined at 700 °C. Similar to Ni-containing aluminas, the alumina-supported Mg, Ca, Ti, and Cr oxides exhibited ordered mesoporosity, large pore widths, and high specific surface area (Table S1 in the Supporting Information). The wide angle XRD patterns (Figure 8) show the presence of $MgAl_2O_4$ spinel (JCPDS 1-87-0345) and alumina phases (JCPDS 50-741 for MA-10Cr-900; JCPDS 1-80-956 for MA-10Ca-900; JCPDS 1-77-396 for MA-10Ti-900) for the Mg-, Ca-, Ti-, and Cr-containing aluminas; note that these data do not exclude the presence of small domains of mixed oxide phases, which cannot be detected by powder XRD. Figure S9 of the Supporting Information presents a photograph of the aforementioned alumina-supported metal oxides to show their color. As expected Mg-, Ca-, and Ti-containing alumina samples calcined at temperatures of 700 and 900 °C are white, while those with chromium oxide are brownish-green.

Conclusions

The proposed one-pot synthesis of alumina-supported metal oxides in ethanol (an environmentally friendly solvent[42]) is facile and applicable for various metals such as Mg, Ca, Ni, Ti, and Cr. The resulting oxides subjected to calcination at temperatures between 400 and 900 °C exhibited high surface area (most often between 200 and 300 m^2/g), large pore widths (8−11 nm), relatively large pore volume (0.3−0.7 cm^3/g), and ordered mesoporosity. Self-assembly of metal and aluminum precursors in the presence of a triblock copolymer structure directing agent followed by controlled calcination afforded nanocrystalline double oxides, often having spinel structure, even at low molar fractions of metal. Those samples with up to ~20% of metal oxide exhibited ordered mesoporosity, a relatively high degree of crystallinity (for samples calcined at temperatures 700 °C and higher), and a homogeneous distribution of metal species. They are thermally stable up to 900 °C, which makes them excellent candidates for catalytic applications.

Supporting Information Available: Adsorption isotherms, PSDs, small angle and wide angle powder XRD patterns, and TEM images for Al_2O_3 samples; TEM images and EDX spectra for MA-10Ni-700; photograph of all MA-10Me samples; ^{27}Al NMR spectra; table listing adsorption parameters for Mg-, Ca-, Ti-, and Cr-containing alumina samples. This material is available free of charge via the Internet at http://pubs.acs.org.

JA806429Q

(40) Sasi, B.; Gopchandran, K. G. *Nanotechnology* **2007**, *18*, 115613–115621.

(41) Sasi, B.; Gopchandran, K. G.; Manoj, P. K.; Koshy, P.; Prabhakara, R. P.; Vaidyan, V. K. *Vacuum* **2002**, *68*, 149–154.

(42) Capello, C.; Fischer, U.; Hungerbuhler, K. *Green Chem.* **2007**, *9*, 927–934.

(43) Ozawa, T. C.; Kang, S. J. *J. Appl. Crystallogr.* **2004**, *37*, 679.